MODELING FLUID COMPOSITION IN CO_2 SATURATED SANDSTONE USING STATISTICAL ROCK PHYSICS, CRANFIELD FIELD, CRANFIELD, MS

Russell W. Carter

Department of Geological Sciences
The University of Texas at Austin

ABSTRACT

Analysis of the effects of injected CO_2 on the seismic response of reservoirs is important because it can provide improved characterization and monitoring of sites undergoing CO_2 injection. In this study we completed a joint inversion of the contact cement model to better understand the effect of CO_2 saturation on the relationship between elastic parameters and reservoir properties of the Cranfield reservoir. We used p-impedance and the Vp/Vs of well logs to invert the rock physics model for porosity and then jointly for porosity and fluid composition. We calibrated a rock physics model to well data from the Cranfield reservoir interval. For the contact cement model to bound the data and correctly model porosity at the Cranfield reservoir, a p-wave coefficient of 1.11 was needed. This term is analogous to a pressure coefficient and simulates increased velocity associated with overburden pressure. We then performed fluid substitution to model density and velocity logs for different in situ CO_2 saturations. The logs, calculated to have a uniform pore fluid composition for all depth points, were input into the inverted model to generate modeled logs of CO_2 saturation and porosity. Results indicated that the model was relatively accurate when inverted for just porosity. Joint inversion for porosity and pore fluid composition predicted porosity successfully but was not able to give as accurate of a prediction of fluid composition. The seismic response of this reservoir is relatively insensitive to fluid saturation so a weighting coefficient may be needed to improve accuracy of fluid modeling.

INTRODUCTION

Geologic storage and sequestration of CO_2 has the potential to help increase oil production from mature fields in addition to contributing to the reduction of anthropogenic CO_2 released into the atmosphere. Recent studies have shown that injected CO_2 can be accommodated in brine and depleted hydrocarbon reservoirs. This potential has been shown at various sites around the world including Snøhvit (Grude et al., 2012), Weyburn (Ma and Morozov, 2009 and Verdon et al., 2010), and Krechba (Mathieson et al., 2010). Regardless of the field location, an important aspect is to monitor the volume and location of injected CO_2 to insure secure storage.

Remote sensing techniques, in particular surface seismic methods, potentially can provide some of this monitoring capability over large-scale areas where dense well bore coverage would be uneconomical or impractical. Time-lapse seismic techniques may allow for monitoring the lateral extent and changing spatial distribution of injected CO_2 over many years.

Research focused on monitoring and characterizing injected CO_2 from time lapse surface seismic data and well logs has been competed by a number of different researchers. Chadwick et al. (2010) quantitatively analyzed multiple vintages of data from the Sleipner field and applied a prestack stratigraphic inversion algorithm and compared it to poststack inversion methods. Prestack inversion better characterized thin intra-reservoir mudstone and sand layers compared to using poststack inversion. Grude et al., (2012) used partial stack time-lapse offshore surface seismic data to help differentiate between fluid saturation effects and pressure effects caused by injection of CO_2 at the Snøvit field offshore Norway. Their findings indicate that in noncemented sandstone reservoirs it is possible to differentiate between the injected CO_2 plume and the pressure front using their technique. Ghaderi and Landrø (2009) examined time-lapse amplitude and travel time shifts to estimate thickness and velocity changes in the Sleipner field. It was found that when combined, 4-D amplitude and time shifts could be used to discriminate between changes in thickness and velocity changes in CO_2 layers in sand beds. More recently, Daley et al. (2011) compared modeled and measured cross-well seismic data to model properties of an injected CO_2 plume at the Frio-II project and generated updated flow models from the relatively high-resolution cross-well seismic observations.

Joint inversion techniques have been used successfully with rock physics models to help characterize hydrocarbons, porosity, and lithology (Bachrach, 2006; Spikes et al., 2007; Spikes, 2008; and Avseth and Norunn, 2011, Jiang and Spikes, 2012). Spikes et al. (2007) used calibrated rock-physics models, surface seismic data, and well log data from offshore South Africa to predict porosity, clay content, and water saturation within the target reservoir. The study found that at the locations of interest, and with a constant thickness assumption for the target reservoir, that the joint inversion method used tended to over predict porosity and gave uncertain predictions of clay and water saturation. A prior study (Bachrach, 2006) used rock physics, stochastic modeling, and a Bayesian estimation method to generate porosity and fluid-saturation maps of expected pay sands. The study used data from both surface seismic and well logs and found that the uncertainty associated with estimations of porosity and the uncertainty of the associated water saturation value are directly correlated. Joint inversion of rock-physics models for reservoir properties was also used by Jiang and Spikes (2012) in their recent work on the Haynesville shale. Their work inverted the self-consistent model for porosity and pore shape. They found that a properly calibrated rock physics model, when inverted, could generate probabilistic porosity and pore shape distributions from measured well logs. These studies

primarily focused on inverting rock physics models for lithological parameters or fluid content based on rock physics model and elastic parameters gathered from well logs.

Inversion of rock physics models has expanded beyond using strictly elastic properties. A recent study included electrical resistivity parameters to simulate monitoring of CO_2 injection (Chen and Hoversten, 2012). Moyano et al. (2011) looked at calibration of rock physics models and found that the accuracy of rock physics modeling could be improved with more rigorous model calibration and quantitative analysis. Uncertainty has the potential to be an issue within quantitative seismic interpretation Grana et al. (2012). It was found by Grana et al. (2012) that uncertainty in inversion methods can be characterize from the initial well log measurements through to the estimated properties of the reservoir. These studies have shown rock physics modeling to be a viable way to relate seismic measurements to reservoir and fluid properties of interest. This study moves to adapt some of these techniques for use in a reservoir undergoing CO_2 injection for storage and utilization purposes.

This study differs from previous studies in that it integrates probabilistic joint inversion of rock physics models and fluid substitution to help differentiate between brine and injected CO_2 in the reservoir. Data for this work comes from the Cranfield reservoir located in Cranfield, MS. These data consist of well logs from both injection and monitoring wells, as well as multiple vintages of surface seismic data and 3-D and time-lapse VSP data. For this study only the pre injection well log data was used. This study builds on the work completed by Carter and Spikes (2013) who examined well logs from the Cranfield area and analyzed them to determine which combinations of parameters gave the highest probability to differentiate between CO_2 and brine in the pore space. A combination of Ip and Vp/Vs were the best performing elastic properties. The world presented here uses that combination as a starting point to invert jointly porosity and fluid saturation using the contact cement model.

DATASET

The Cranfield reservoir consists of sandstones of the Lower Tuscaloosa Formation, which has been dated regionally to be Upper Cretaceous in age. The reservoir sands of the Cranfield study area have porosities that range from 0 to 37% with an average value of 20% (Lu, et al., 2012). Permeabilities in the reservoir range from 0.1–1000 millidarcies (Lu et al., 2012). The Late Cretaceous Tuscaloosa group contains alternating sequences of sands and shales that comprise the reservoir and the reservoir seals, respectively, in the study area. An extensive regional scale marine shale is present in the Middle Tuscaloosa Formation that acts as a regional seal to the reservoir sands. The Cranfield study area is near the apex of a local anticline, which is being forced upward through the buoyant rising of a salt body (Lu et al., 2012).

The Cranfield reservoir was produced from discovery in 1943 until its initial abandonment in 1966. The site has since been revived as a location for enhanced oil recovery and CO_2 injection and sequestration. The site was selected due to its proximity to regional infrastructure, regionally available CO_2 and the high possibility of economically recoverable hydrocarbon reserves through the use of CO_2 based EOR (Lu et al, 2012). The Gulf Coast Carbon Center at the University of Texas at Austin Bureau of Economic Geology is working with the Southeast Regional Carbon Sequestration Partnership as well as the local field operator to conduct the CO_2 sequestration study at the Cranfield site (Lu et al., 2012). The study area is located with in the 1 km^2 Detail Area Study (DAS), contained with in the red box on Figure 1. The DAS consists of three wells, one injection well, CFU-31F-1 (F-1) and two monitoring wells, CFU-31F-2 (F-2) and CFU-31F-3 (F-3), which are located down structural dip from the injection well. During CO_2 injection, injection rates into well F-1 ranged between 200 and 500 tons per day. Over the entire Cranfield area more than 3.4 million tons of CO_2 have been injected in total.

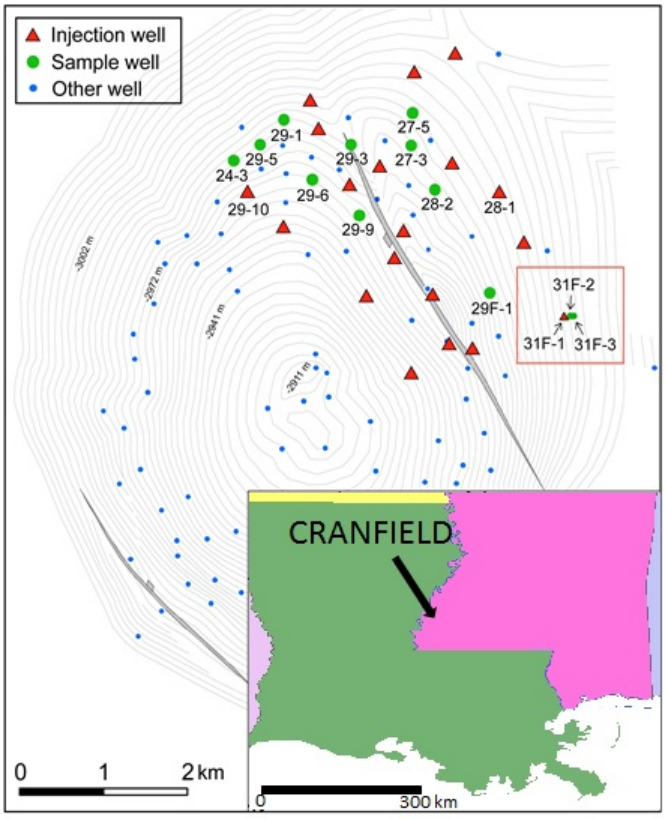

Figure 1. The entire Cranfield site. Data for this project came from the DAS (red box). The DAS contains one injection well, 31F-1 (F-1), and two monitoring wells, 31F-2 (F-2) and 31F-3 (F-3). Modified from Lu et al. (2012).

Logs from well F-2 before injection commenced are shown in Figure 2. Panels a, b, and c show the Vp, Vs and gamma ray logs respectively. The reservoir zone in well F-2 can be broken down into two district zones. The upper reservoir zone shown in red ranges from 3184 to 3194 meters and the lower reservoir zone, shown in green extends from 3196 to 3201 meters. The gamma ray log (panel c) shows an increase in gamma ray count at 3195 meters and indicates a local shale layer that divides the upper and lower reservoir zones.

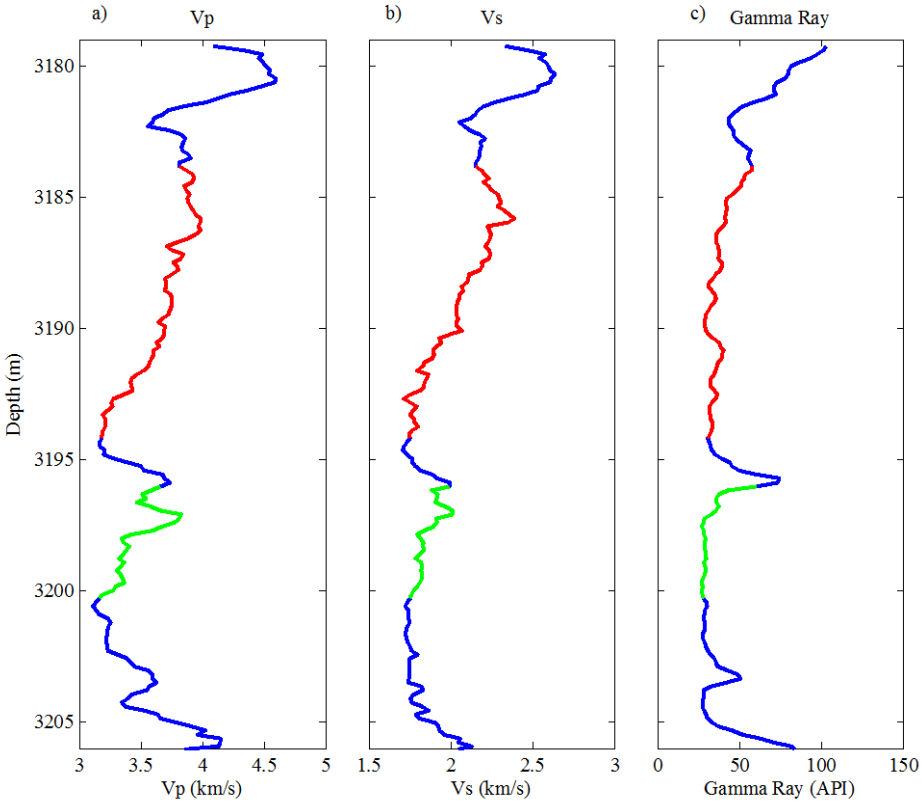

Figure 2. Well F-2. The red line shows the shallower reservoir zone, which extends from about 3184 to 3194 m, and the green line shows the deeper reservoir zero, which extends from about 3196 to 3201 m. The shale layer that divides the two reservoir zones is apparent from the increase in the gamma ray count between 3194 and 3196 ft.

Theory and Methods

This study is a multi-step process that builds on the results and finding of previous work completed by Carter and Spikes (2013) who found that Vp/Vs is a useful parameter to discriminate fluid saturation. In this study a rock physics model is used to link reservoir properties to the elastic parameters of the reservoir. Elastic parameters calculated from measured

well logs and from well logs modified by fluid substitution are then used to invert the rock physics model to generate probabilistic logs of porosity and fluid saturation in the reservoir.

Rock Physics Modeling

Contact theory models are a subset of rock-physics models that are based on the assumption that the stiffness of a rock is related to the stiffness of the individual grains, the number of grain contacts, and the stiffness and amount of cement that is present at grain contacts (Dvorkin et al., 1994 and Dvorkin and Nur, 1996). The contact cement model, the model used in this study, is derived from Hertz-Mindlin theory (Mindlin, 1949). During the derivation of the contact cement model, a grain contact cement term was included in the model; however, the pressure term of the model was dropped. In the derivation, the inclusion of cement between two grains under compression reduces to a linear integral regression where the stiffness of the cemented grains does not depend on confining pressure (Dvorkin et al., 1991). In the contact cement model, porosity of the rock decreases directly with an increase in the amount of contact cement because cement is being deposited in the existing pore space of the rock frame. Cement in this model can be deposited in two different ways as is shown with the dark and light blue lines in Figure 3. The first method is to deposit the cement evenly and concentrically around each grain. This depositional geometry corresponds to the light blue line of Figure 3. The second method of cement formation is that cement is deposited only at grain contacts. The dark blue line of Figure 3 illustrates this depositional geometry. For rock-physics modeling purposes this study used the first method of cement deposition (light blue line Figure 3).

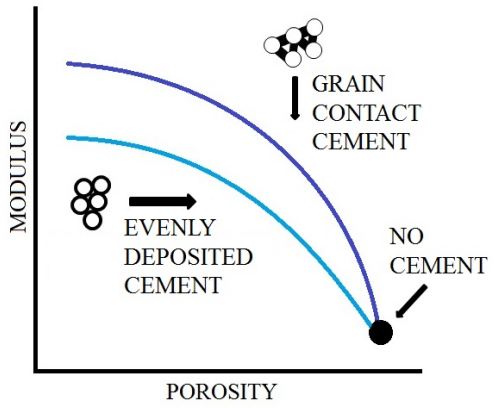

Figure 3. A schematic of the contact cement model. Cement can be deposited concentrically around the grain following the lower path on the graph or only at grain contacts, following the upper line on the graph. As cementation increases, porosity decreases, and the elastic moduli increase.

Previous work conducted at this same location and on the F-2 well have shown that the reservoir interval is composed primarily of 60-80% quartz, 10-20% clay, and 10-20% feldspar, with the remainder composed of small percentages of muscovite, calcite, and other minerals (Kordi et al., 2010). Initial rock physics work done at this location by Carter and Spikes (2013) used a single composition of 61% quartz, 18% clay, 17% feldspar, 3% muscovite, and 1% calcite to represent the mineral grain in the rock physics model. Given the natural heterogeneity present in the reservoir and the range of composition percentages shown by Kordi et al. (2012) the rock physics model was expanded to cover a wider range of mineral compositions. The expanded set of contact cement compositions was selected to be geologically consistent with the work completed by Kordi et al., (2012). To complete this we computed the contact cement model 50 times for a range of mineral compositions, ranging from 40% quartz and 60% clay to 100% quartz. Intermediate composition also contained fractions of feldspar, and calcite.

During the derivation of the contact cement model the pressure term is dropped. However, modeling the Cranfield reservoir with the contact cement model in a way that is consistent with known geology tended to generate a mismatch between the known measured porosity at the well location and the porosities predicted by the contact cement model. It has been shown by numerous studies (Nur and Simmons, 1969; Nur, 1971, Sayers, 1988; and Mavko et al, 1995) that an increase in confining pressure can cause an increase in seismic velocity due to an increase in intergranular friction and closing of pores and cracks. Alignment of the modeled porosity with the measured porosity required an 11% increase in the modeled p-wave velocity. This is consistent with the increase in velocity measured by Joy (2011) on core plugs from the Cranfield reservoir under pressure. The measurements taken by Joy (2011) showed that p-wave velocity through core samples from the Cranfield reservoir increased in velocity nonlinearly with an increase in pressure. For pressures anticipated at 3100 to 3200 meters depth, an increase in p-wave velocity in the range of 11% is anticipated. Shear wave velocities were not increased to compensate for pressure because the measurements by Joy (2011) show that s-wave velocities, do not increase with increasing pressure as much as the p-wave values do.

It has been shown for this reservoir that p-impedance and Vp/Vs ratio was the parameter combination that best discriminated between different fluid compositions (Carter and Spikes, 2013). By modeling the contact cement model for all porosities between critical porosity and zero porosity, with pore fluids composition ranging from pure brine to pure CO_2 for each porosity value, the response of the model to fluid saturation can be examined. This model was initially run with a fixed lithology for calibration purposes. Figure 4 shows the contact cement model generated for a fixed lithology of pure quartz, but the pore fluid ranges from pure brine to pure CO_2. Panel a of Figure 4 shows the contact cement model colored by porosity, with porosity being primarily a function of Ip. Panel b of Figure 4 shows the same model color coded

to pore fluid with dark blues corresponding to pure CO_2 and red to pure brine. Panel b demonstrates that pore fluid is primarily a function of the Vp/Vs ratio.

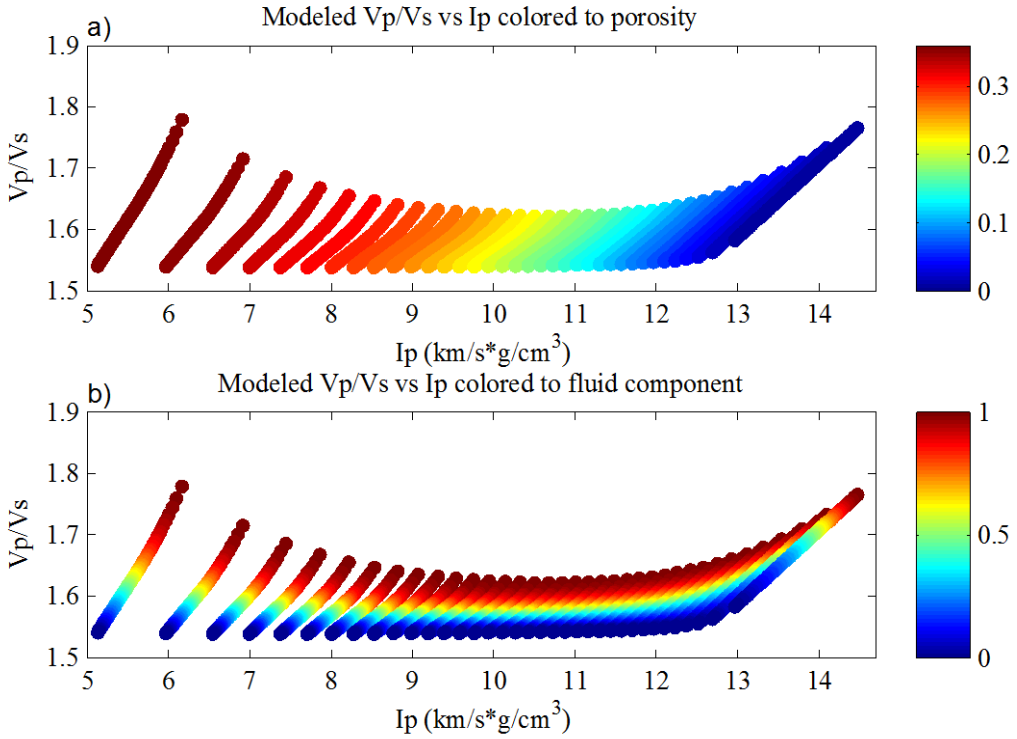

Figure 4. Example illustrating modeled Vp/Vs vs p–Impedance (Ip) calculated from the contact cement model. This model is based on single lithology of a pure quartz grain with clay contact cement. In panel a) the model is colored to porosity. In panel b) the model is colored to water saturation (Sw), with the remainder of the pore fluid composed of CO_2. For this model the fluids were mixed according to the Voigt upper bound. Porosity differentiation tends to be a function of primarily Ip whereas water saturation discrimination is primarily a function of Vp/Vs.

Modeled trends from the contact cement model with the pressure correction are shown in Figure 5. Figure 5a shows the contact cement model for the 50 different lithologies and for the full range of pore fluid composition between pure brine and pure CO_2. Colors in panel a indicate porosity and the black data points shown are the measured well log data. Panel b of Figure 5 shows the same information as Panel a with the measured data being colored to porosity and the modeled data being shown in black. The color scales for both panels a and b are the same with red and other warm colors indicating high porosity and blue and other cool colors indicating relatively low porosity. This figure shows that for a given Vp/Vs and Ip value the modeled porosity correlates closely with the measured porosity. Additionally it shows that the model does a good job of covering the range of Vp/Vs and Ip values that are represented in the data.

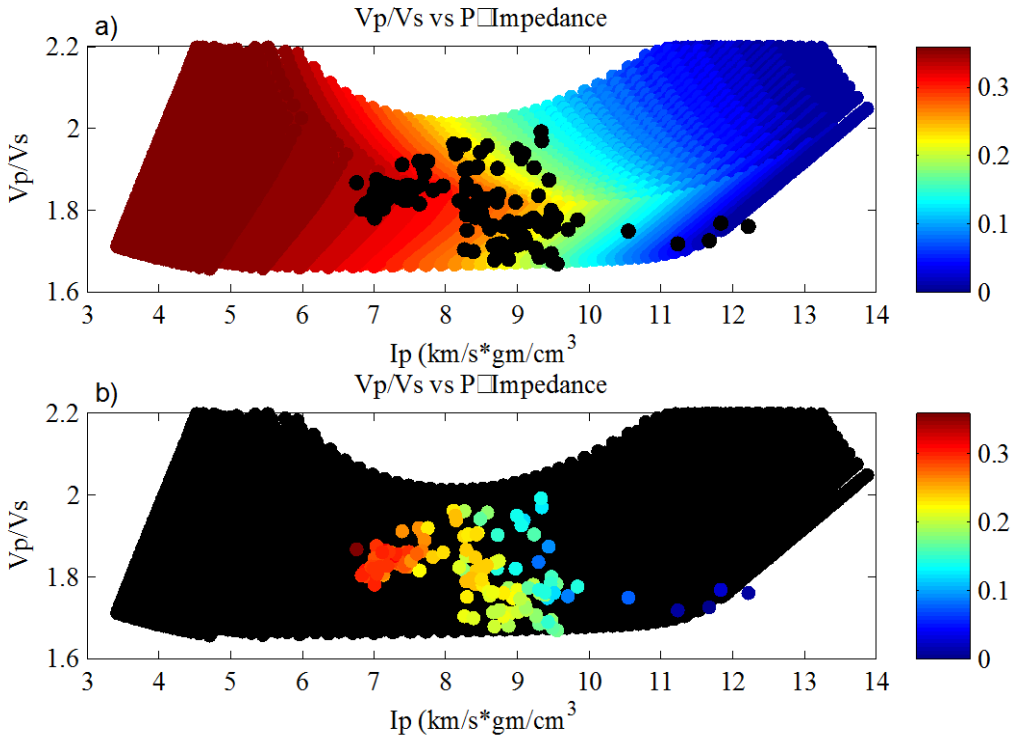

Figure 5. Modeled Vp/Vs vs p–Impedance (Ip) with well log measurements color coded to porosity. Both panels a and b show Vp/Vs on the y-axis and the p-impedance (Ip) on the x-axis. In panel a the colored data points show the results of the contact cement model for 50 different lithologies each modeled for the full range of pore fluids between pure brine and pure CO_2. The scattered black data points are measured log data. Shading in panel a shows porosity of the contact cement model results. Panel b shows the same information as panel a, however, the measured data points are shaded by porosity and the modeled data is shown in black. Shading in both panels is to the same scale with warm colors indicating relatively high porosity and cool colors indicating low porosity.

Joint Inversion

The first step of the joint inversion was to compute the models from which to generate the relationships between elastic parameters and reservoir properties. This was done by taking the contact cement models for the range of different mineralogies shown in Figure 4 and completing fluid substitution analysis on them. As a result, each different lithology was modeled for the range of pore fluid compositions between pure brine and pure CO_2. Data from all the different lithologies and fluid compositions were then binned for certain ranges of impedance and Vp/Vs. For this study modeled data was divided into 225 bins, with fifteen divisions along the impedance axis and fifteen divisions along the Vp/Vs axis. Gaussian bivariate probability density functions were generated for each of the 225 bins. These bivariate probability density functions provided a statistical relationship between porosity and fluid saturation for each bin. These

probability density functions show the highest probability combinations of porosity and pore fluid for the range of Ip and Vp/Vs within each bin. An example of these probability density functions is shown in Figure 6. In Figure 6, porosity is shown along the x-axis and pore fluid composition is shown along the y-axis with color representing probability. Black and red show high probability and white and light yellow show areas of relatively low or zero porosity, respectively.

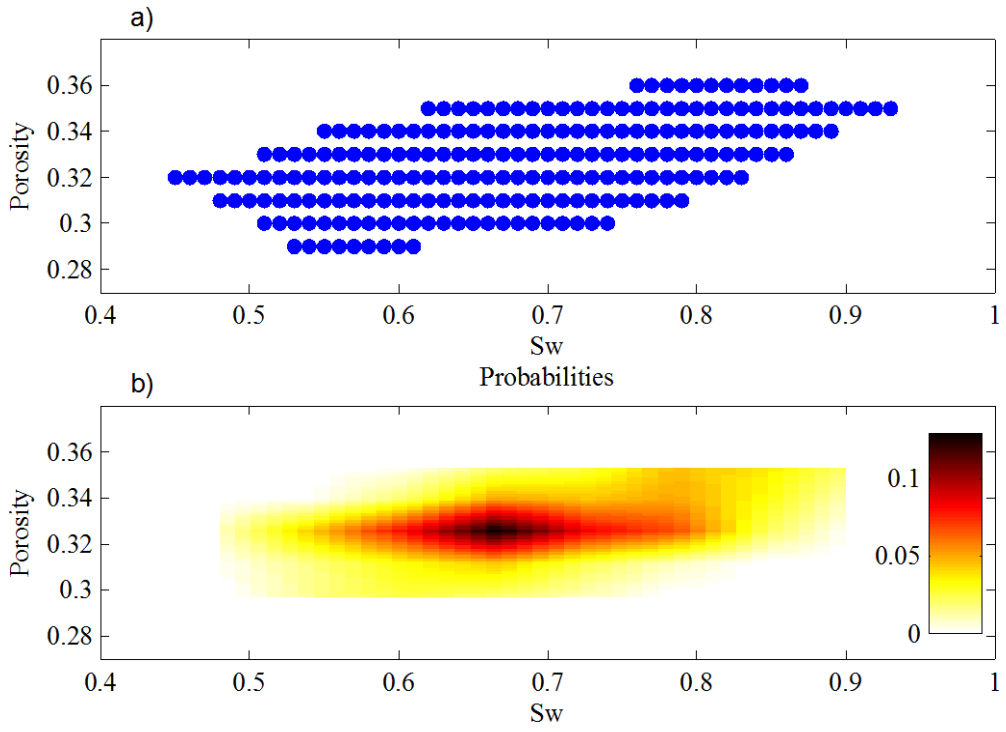

Figure 6. Both panels of Figure 6 show water saturation along the x-axis and porosity along the y-axis. Panel a of the figure shows the data points from all lithology variations of the fluid saturated contact cement model that fell into the selected Ip and Vp/Vs range of 5.45 to 6.24 and 1.81 to 1.87, respectively. Panel b of the figure shows the PDF of the data points in panel a, with dark red and black regions showing a high density of data points and light yellow and white show a low density of data points.

With all the contact cement models binned, the measured well log data, calculated to represent a uniform fluid composition, was then also binned according to the same Ip and Vp/Vs bins as the model data. When the entire reservoir section of the well log was binned, 500 joint normally distributed porosity and pore fluid values were assigned to each depth point. This number of joint values was chosen for each combination of Ip and Vp/Vs to examine the full extent of the potential variability and to generate a probabilistic output of porosity and pore fluid. By calculating 500 bivariate values for each depth point, probabilistic logs of porosity and fluid saturation were generated. These logs showed the highest probability outcome of porosity and

pore fluid composition given the input Ip and Vp/Vs for a single depth point. The joint values generated for each bin of measured values of Vp/Vs and Ip were selected to have the same mean, standard deviation, and covariance as the Vp/Vs and Ip results of the contact cement model for the same bin values. This was completed once for the measured Ip and Vp/Vs with each of the following fluid compositions: 0, 25, and 50% CO_2, with the remainder of the pore fluid composed of brine. Measured logs were fluid substituted to the pore fluids of 0, 25 and 50% CO_2 using Gassmann (1951) fluid substitution. This was not completed for 75% and 100% CO_2 because CO_2 saturations of that amount were not expected in the reservoir except perhaps directly around the injection well.

After the porosity and pore fluid logs were generated, they were smoothed to mimic spatial relationships between adjacent depth points. A range of smoothing values was tested to determine how much smoothing was needed to best match between the measured porosity logs and modeled porosity logs. Smoothing was accomplished by applying a moving average to the output porosity values. A two-point moving average window averaged one depth point with the following depth point whereas a five and ten point moving average averaged one depth point with the five and ten, respectively, successive depth points. Smoothing values of two and ten were chose to represent the minimum possible smoothing, two, and what was anticipated to be excessive smoothing, with a ten point moving average.

RESULTS

Porosity Inversion

As an interim step the well log data was initially inverted just for porosity. Inverting for porosity was completed to confirm that the model was working and to help determine the necessary degree of smoothing. The results from the probabilistic porosity inversion returned a porosity output that tended to follow the trends of the measured data (Figure 7a) when no smoothing was applied. In all panels of Figure 7, the x-axis indicates porosity and the y-axis shows depth in meters. The blue line indicates the measured porosity values, and the shaded region shows the probability of the modeled porosity values being less than the porosity value at that point and color combination. The black regions corresponds to a P-50 value of porosity, and the white and light yellow shaded regions on the left and right of the black shaded region correspond to the P-10 and P-90 values, respectively.

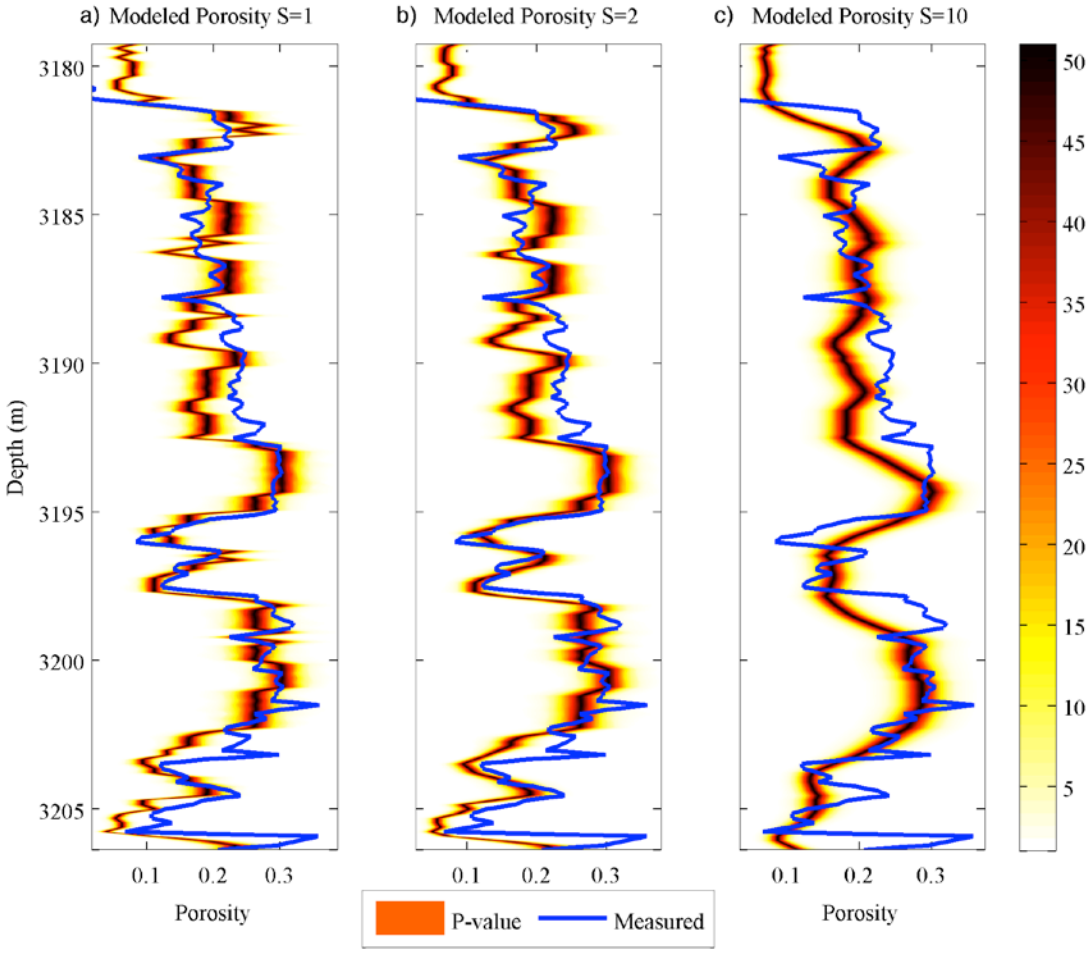

Figure 7. Inverted porosity from the rock physics model using Vp/Vs and Ip as input parameters. The blue line in each panel represents the measured porosity value. The shaded region in each panel indicates the range of mapped porosities and the color of the shading indicates the probability of a specific mapped porosity value for a given depth point from 500 simulations. Values to the left of the P-50 (black) line are P-0 through P-50. Values to the right of the P-50 line show P values ranging from P-50 to P-100. Panel a) shows modeled data with no smoothing, panel b) shows calculated data with a two-point window. Panel c) shows increase smoothing with a ten-point window.

Modeled porosity in this initial test followed the general trends of the measured data. However, the output porosity values from the joint inversion showed variations between depth points that were not present in the measured data. To minimize this inherent variation that resulted from the joint inversion, two different degrees of smoothing were applied to the modeled logs. In Figure 7b the modeled porosity values were smoothed over two consecutive depth points. Panel c of Figure 7, shows the same data again. However, in panel c the modeled porosity was smoothed over ten depth points by applying a ten point windowed moving average

to the output porosity data. In Figure 7c the modeled values are over smoothed. With a simple two point moving average (Figure 7b) applied to the modeled data, much of the point-by-point variation that was present in the nonsmoothed data was removed, giving a more reliable fit of the modeled data to the measured data. Results from this initial study show that inversion of the contact cement model for porosity at this location returns a porosity log that closely matches the measured porosity. Additionally the optimal degree of smoothing to match the model to the input porosity logs is achieved by using a two point windowed moving average.

Joint Inversion

Joint inversion for porosity and fluid saturation was performed on the results of the contact cement model run for 50 different lithologies. Each lithology combination was then fluid substituted for the full range of pore-fluid compositions ranging from pure brine to pure CO_2. Five hundred porosity and fluid combinations were then generated to be statistically equivalent for a range of measured Vp/Vs and Ip values modeled values from the contact cement model. Measured input data for the joint inversion had fluid replacement done on it to bring the input fluid to pure brine to allow for verifying the accuracy of the inversion for fluid composition. Figure 8 shows the results of the initial joint inversion where the input Ip and Vp/Vs values were those generated from the measured logs with pore fluid modeled to be pure brine. Panel a shows the results of the porosity inversion, and panel b shows the results of the inversion for pore-fluid composition. In panels a and b the x-axis is porosity and water saturation, respectively. In both panels the vertical axis is depth, and the blue line represents measured data that has been recalculated to a constant pore fluid. The shaded region of both panels is the probability of the inversion results returning a given value for a certain depth point. Black and dark red correspond to approximately a P-50 value and light yellow to a P-10 and P-90 valued on the left and right of the P-50 value, respectively. In this figure the inverted results for porosity and fluid saturation have been smoothed by a two point moving average.

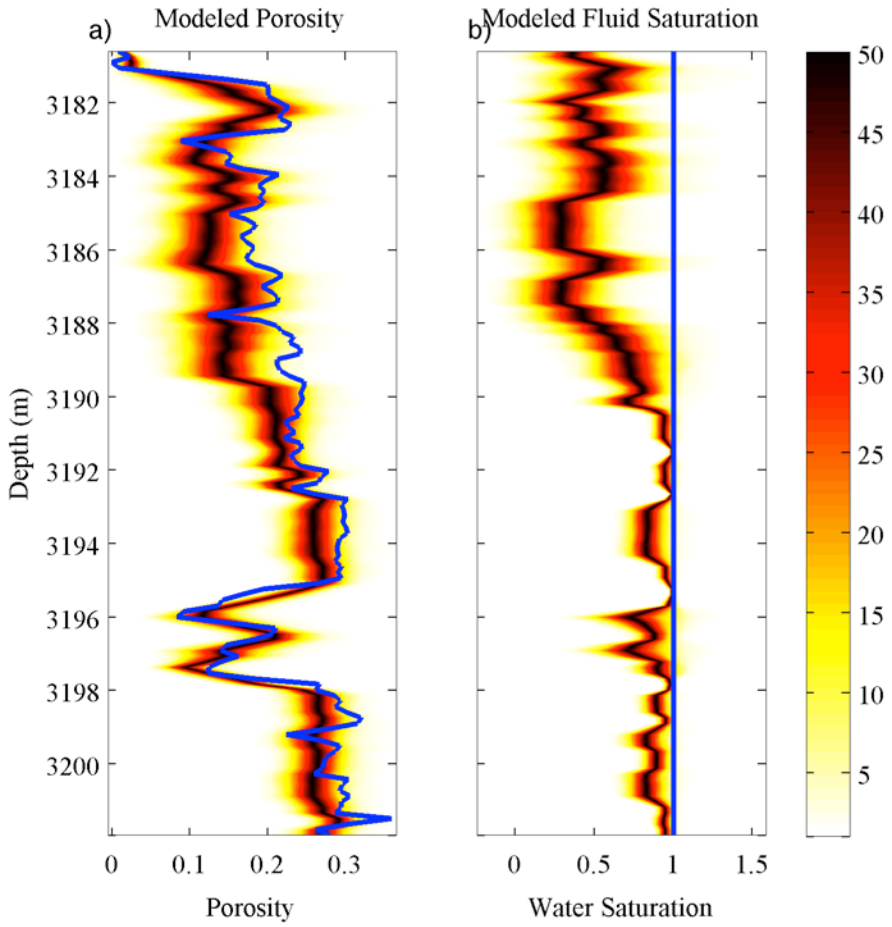

Figure 8. Results of the joint inversion for porosity and water saturation. Panel a) shows the porosity result, and panel b) shows the fluid saturation result. The blue line represents measured porosity and the fluid saturation for panel a) and panel b), respectively. The colored region in each panel represents the probability of a given porosity or saturation value being generated for a given depth point. Inverted data in both panels has had a two point moving average applied for smoothing.

Figure 8 shows that the joint inversion tended to predict porosity for the most of the reservoir zone with a relatively high degree of accuracy. However, the joint inversion did tend to slightly over predict porosity while still showing a similar trend to the measured data for the majority of the reservoir zone. In panel b the inverted pore fluid values show a relatively constant trend for the deeper portion of the reservoir, which gives a modeled fluid saturation that is similar to the input saturation. In the shallower portion of the reservoir (above 3190 meters) the predicted pore fluid values show a higher concentration of CO_2 than the input data, while also showing significantly more variability than was present in the input data.

This same process was completed again for a pore fluid compositions of 75% brine and 25% CO_2 (Figure 9) and for a pore fluid composition of 50% brine and 50% CO_2 (Figure 10). For both Figure 9 and Figure 10, panels a and panels b show depth on the y-axis and porosity and water saturation on the x-axis, respectively. The shaded region in each panel shows the probability of the predicted value at that depth point, with white and light yellow approximating the P-10 and P-90 values on the left and right of the P-50 value (black and dark red line), respectively. The blue line in both panels shows the measured, fluid substitution input data for the joint inversion. Results from both Figures 9 and 10 are similar to those shown in Figure 8. Porosity prediction from the joint inversion showed parallel trending to and a relatively accurate model below a depth of 3190 meters. At depth shallower than 3190 meters the modeled porosity in Figures 9 and 10, while showing parallel trends, are slightly under predicted relative to the input data. For pore fluid prediction, the results from the joint inversion tended to return relatively similar results for all three fluid situations in the shallower portion, above 3190 meters, of the reservoir. For the deeper portion of the reservoir the modeled fluid shows increasing variability with increasing CO_2 concentration in the input logs. Along with this increasing variability is an increase in predicted CO_2. Despite the increase in predicted CO_2 with increased CO_2 concentration on the input logs, the results do not provide an accurate and reliable estimate of CO_2 concentration in the pore space at this scale.

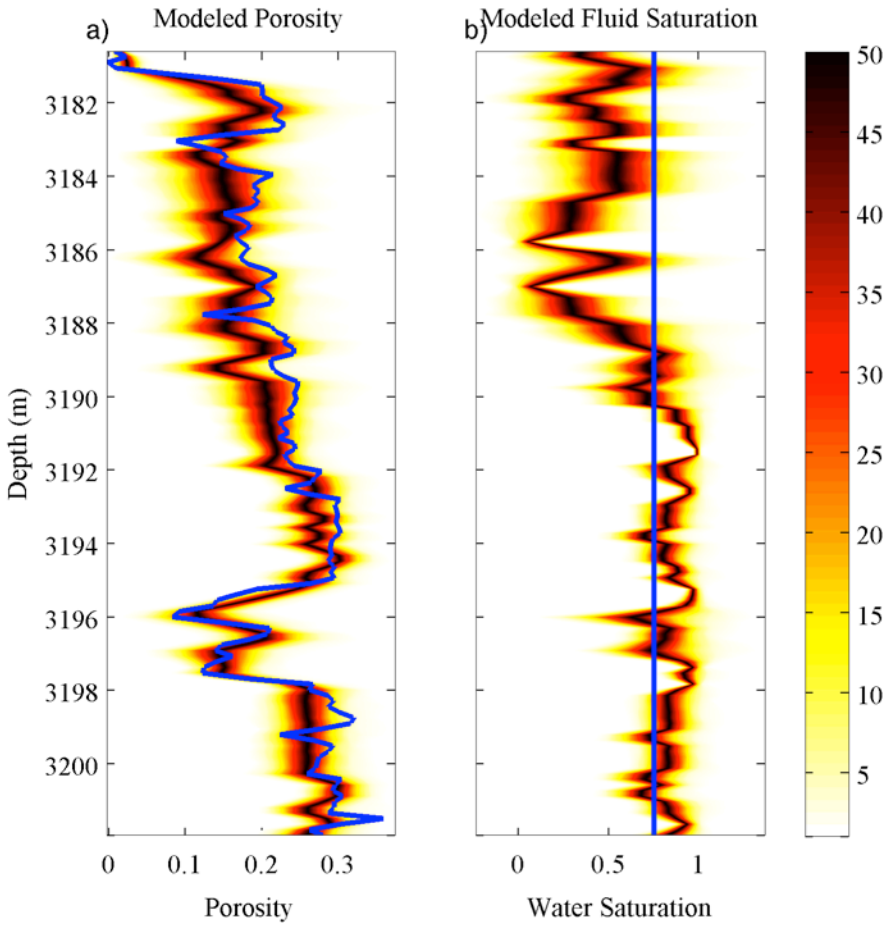

Figure 9. Results of the joint inversion for porosity and water saturation, with the input data corresponding to a fluid that is 75% brine and 25% CO_2. Panel a) and b) show the results of the porosity and fluid saturation inversion, respectively. The colored region in each panel represents the probability of a given porosity or saturation value being mapped for a given depth point. The blue line represents measured porosity and the fluid saturation for panel a) and panel b), respectively.

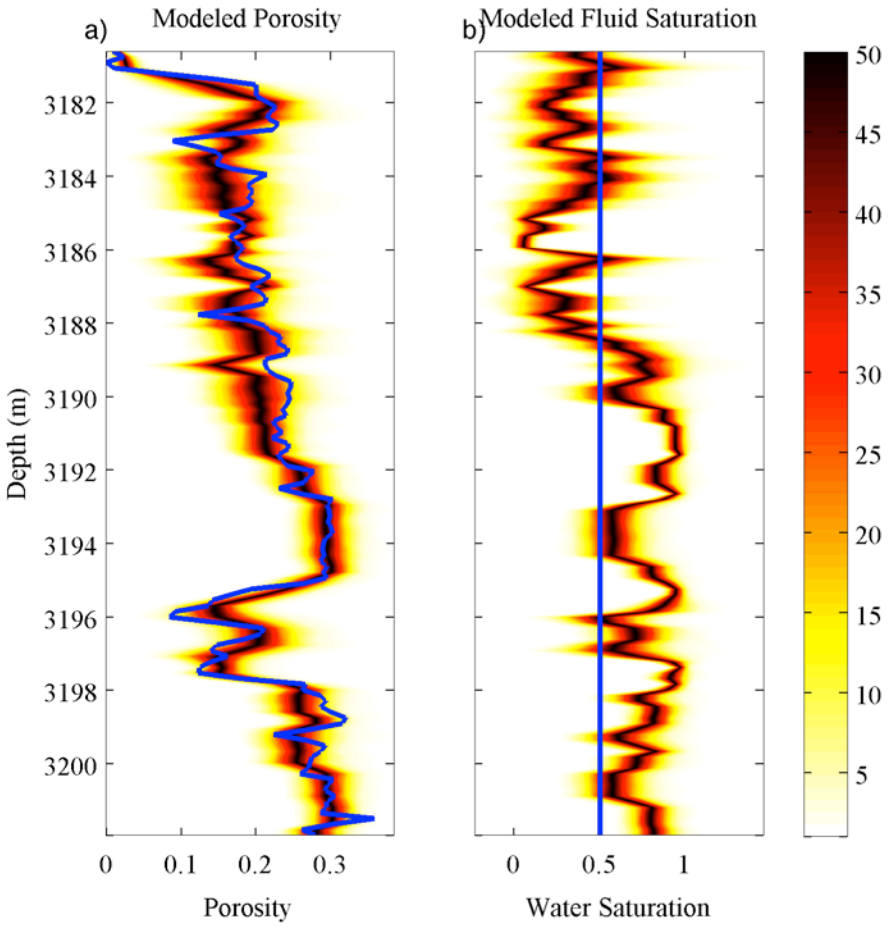

Figure 10. Results of the joint inversion for porosity and water saturation are shown in panels a) and b), respectively. The blue line shown in both panels shows the porosity and pore fluid composition for the input data in panels a) and b), respectively. The colored region in each panel represents the probability of a given porosity or saturation value being generated for a given depth point. Input CO_2 in the model has been set to a constant 50% with the remainder of the pore fluid being brine. Because of the influence of Vp on both Ip and Vp/Vs there is some parallel trending in the porosity and water saturation logs. This is most apparent at 3196 and 3199 meters in depth.

DISCUSSION

As expected the results from the Ip and Vp/Vs inversion for a single parameter returned an estimate of porosity that was relatively well constrained, compared to the joint inversion for porosity and water saturation. Additionally, the inversion for just porosity returned results that matched the measured porosity in the reservoir fairly closely. The joint inversion did not return a porosity values that matched the input values, as well. Using two measured parameters (Ip and Vp/Vs, in this study) to invert for a single parameter leads to an over determined problem. An over determined problem helps to increase the state of knowledge with respect to the unknown

parameter, in this case porosity, relative to the state of knowledge of the unknown in a equally determined problem (Takahashi, 2000). This also holds true when inverting two parameters for two unknowns where the state of knowledge is decreased relative to inverting for a single parameter (Takashahi, 2000). When comparing the range of possible output values in the probabilistic inversion of the inverted porosity log (Figure 7) to the probabilistic porosity log from the joint inversion (Figure 8), it can be seen that the range of porosities for any given depth point is much larger in Figure 8. This is due the non-uniqueness of the porosity/saturation combination that could be represented by a given Ip and Vp/Vs ratio. The non-uniqueness for porosity and saturation combinations manifests because of the incomplete state of knowledge generated by the input model (Takahashi, 2000).

The results from the joint inversion returned a porosity log that showed the same trends as the measured porosity values, however there was a slight tendency in the shallower portion of the reservoir to under predict the porosity. Additionally, this work generated water saturation logs that were quite similar regardless of what pore fluid was of the input log. Having one parameter trending fairly accurately while the other logs do not trend accurately was not excepted. It has been shown that in a joint inversion situation the parameters being inverted for tend to be linked (Bachrach, 2006). As such an under prediction of one parameter could lead to either an over prediction or under prediction of the other parameter. However, given that one parameter is fairly accurate, a coefficient on the covariance matrix that generates the bivariate Gaussian random number could improve the accuracy of the modeled fluid saturation values (Bacharach, 2006, Spikes et al., 2008).

In this study a coefficient of 1.11 was multiplied with the modeled p-wave velocities as generated by the contact cement model. As the contact cement model has no pressure dependence the multiplier of 1.11 was used based on the results obtained by Joy (2011). Without a pressure coefficient, the joint inversion of the contact cement model tended to under predict the porosity of the input log. By increasing p-wave velocity with a coefficient Ip was also increased for a given porosity in the model. Consequently, when a given Ip was input into the inverted model, the output porosity was increased as well. Recent studies have started to look at integrating a pressure term into cement inclusive contact theory models (Avseth and Norunn, 2011). Future work could include looking into these models to help constrain and link the coefficient used in this study to an effective pressure at the reservoir.

CONCLUSIONS

This study showed that the contact cement model, can be used to model the Cranfield reservoir for porosity when properly calibrated. However, in this case the properties of the

reservoir are such that the contact cement model tended to under predict the porosity of the reservoir for a given Ip values. At the depth of the Cranfield reservoir, over 3000 meters, the effective pressure is thought to be approximately 30 MPa. Given this effective pressure a p-wave coefficient of 1.11 was required for the contact cement model to correctly link porosity and Ip given the relatively well-constrained lithology of the Cranfield reservoir.

Inversion of Ip and Vp/Vs only for porosity returned a modeled porosity log that displayed the same general trend as the measured porosity values. The joint inversion for both porosity and fluid saturation returned a porosity log that showed a relatively accurate match between input porosity and output porosity. However, the log of modeled pore fluid composition was less accurate for all different pore fluid combinations tested. While the two parameters in joint inversion are linked, it is still possible in this case for one of the modeled parameters to show a relatively high degree of accuracy while the other parameter is modeled with a relatively low degree of accuracy. This indicates that while the two parameters in a joint inversion are linked, it might be necessary to provide a weighting coefficient to ensure accurate results for both parameters being inverted for. The two measurements used in this study are Ip and Vp/Vs. These are both affected by changes in Vp. It was observed that while Ip and Vp/Vs are primarily affected by porosity and fluid saturation, respectively, a small degree of parallel trending may be observed in the modeled results due to their combined reliance on Vp. Additionally the reduced accuracy of the fluid modeling can be, in part, attributed to the low degree of sensitivity of the reservoir to fluid saturation. The addition of a weighting coefficient to mitigate the effects of Vp may also help to amplify the subtle changes in the reservoir properties due to fluid composition and help improve fluid modeling accuracy.

REFERENCES

Avseth, P., Skeji, Norunn., 2011, Rock physics modeling of static and dynamic reservoir properties – a heuristic approach for cemented sandstone reservoirs, The Leading Edge, **30**, 90–96.

Bachrach, R., 2006, Joint estimation of porosity and saturation using rock-physics modeling, Geophysics,**71**, O53–O63.

Carter, R., and Spikes, K., 2013, Sensitivity analysis of Tuscaloosa sandstones to CO_2 saturation, Cranfield field, Cranfield, MS. International Journal of Greenhouse Gas Control, Accepted.

Chadwick, A., Williams, G., Delepine, N., Clochard, V., Labat, K., Sturton, S., Buddensiek, M., Dillen, M., Nickel, M., Lima, A., Arts, R., Neele, F., Rossi, G., 2010. Quantitative analysis of time-lapse seismic monitoring data at the Sleipner CO_2 storage operation. The Leading Edge. **29**, 170–177.

Chen, J., and Hoversten, M., G., 2012, Joint inversion of marine seismic AVA and CSEM data using statistical rock-physcis models and Markov random fields, Geophysics, **77**, R65–R85.

Daley, T. M., Ajo-Franklin, J. B., Doughty, C., 2011. Constraining the reservoir model of an injected CO_2 plume with crosswell CASSM at the Frio-II brine pilot. International Journal of Greenhouse Gas Control. **5**, 1022–1030.

Dvorkin, J., Mavko, G., and Nur, A., 1991, The effects of cementation on the elastic properties of granular material, Mechanics of Materials, **12**, 207–217.

Dvorkin, J., Nur, A., and Yin, H., 1994, Effective properties of cemented granular material, Mechanics of Materials, **18**, 351–366.

Dvorkin, J. and A. Nur, 1996, Elasticity of High-porosity sandstones: Theory for two

North Sea datasets, Geophysics, **61**, 1363–1370.

Gassmann, F., 1951, Uber die elastizitat poroser medien, Vier. Natur Gesellschaft, **96**, 1-23.

Ghaderi, A., Landrø, M., 2009. Estimation of thickness and velocity changes of injected carbon dioxide layers from prestack time-lapse seismic data. Geophysics. **74**, O17–O28.

Grana, D., Pirrone, M., and Mukerji, T., 2012, Quantitative log interpretation and uncertainty propagation of petrophysical properties and facies classification from rock-physics modeling and formation evaluation analysis, Geophysics, **77**, WA45–WA65.

Grude, S., Landrø, M., and Osdal B., 2012, Time lapse seismic interpretation of CO_2 storage at Snøhvit field. EAGE Expanded Abstracts, Third EAGE CO_2 Geologic Storage Workshop.

Jiang, M., and Spikes, K., 2012, Estimation of the Haynesville shale using the Self-Consistent Model and a Grid Search Method, SEG Expanded Abstracts, (Pending publication).

Joy, C., 2011, The effects of pressure variations and chemical reactions on the elasticity of the lower Tuscaloosa sandstone of the Cranfield Field, Mississippi, The University of Texas at Austin Masters Thesis.

Kordi, M., Hovorka, S., Milliken, K., Treviño, R., Lu, J., 2010. Diagenesis and reservoir heterogeneity in the Lower Tuscaloosa Formation at Cranfield Field, Mississippi: presented at the 60th Annual Convention of the Gulf Coast Association of 96 Geological Societies and the Gulf Coast Section of SEPM. San Antonio, Texas. October 10-12, 2010. GCCC Digital Publication Series #10–13.

Lu, J., Kharaka, Y., Thordsen, J., Horita, J., Karamalidis, A., Griffith, C., Hakala, A., Ambats, G., Cole, D., Phelps, Manning, M., T., Cook, P., Hovorka, S., 2012. CO_2–rock–brine interactions in Lower Tuscaloosa Formation at Cranfield CO_2 sequestration site, Mississippi, USA. Chemical Geology. 291, 269–277.

Ma, J., Morozov, I., 2010, AVO modeling of pressure-saturation effects in Weyburn CO_2 sequestration. The Leading Edge. 29, 178–183.

Mavko, G., Mukerji, T., and Godfrey, N., 1995, Predicting stress-induced velocity anisotropy in rocks, geophysics, **60**, 1081–1087.

Mathieson, A., Midgley, J., Dodds, K., Wright, I., Ringrose, P., and Saoul, N., 2010, CO2 sequestration monitoring and verification technologies applied at Krechba, Algeria, The Leading Edge, **29**, 216–222.

Mindlin, R. D., 1949. Compliance of elastic bodies in contact. Journal of Applied Mechanics. **16**, 259–568.

Moyano, B., Jensen., E., H., and Johansen., T., A., 2011, Improved quantitative calibration of rock physics models, Petroleum Geoscience, **17**, 345–354.

Nur, A., 1971, Effects of stress on velocity anisotropy in rocks with cracks, Journal of Geophysical Research, **76**, 2022–2034.

Nur, A., and Simmons, G., 1969, Stress-induced velocity anisotropy in rocks: An experimental study, Journal of Geophysical Research, **74**, 6667.

Sayers, C., M., 1988, Stress-induced ultrasonic wave velocity anisotropy in fractured rock. Ultrasonics, **26**, 311–317.

Spikes, K., 2008, probabilistic seismic inversion based on rock-physics models for reservoir characterization, Stanford University PhD Dissertation.

Spikes, K., Mukerji, T., Dvorkin, J., and Mavko, G., 2007, Probabilistic seismic inversion based on rock-physics models, Geophysics, **72**, R87–R97.

Takahashi, I., 2000, Quantifying information and uncertainty of rock property estimation from seismic data, Stanford University PhD Dissertation.

Verdon, J. P., Kendall, J-M., White, J. D., Angus, D. A., Fisher, Q. J., Urbancic, T., 2010. Passive seismic monitoring of carbon dioxide storage at Weyburn. The Leading Edge. **29**, 208–214.